Piezoelectric Energy Harvesting System

for Low-Power IoT Sensors

Laurens-Jan Cammeraat
Wester Landman

Contains:
Circuit Design

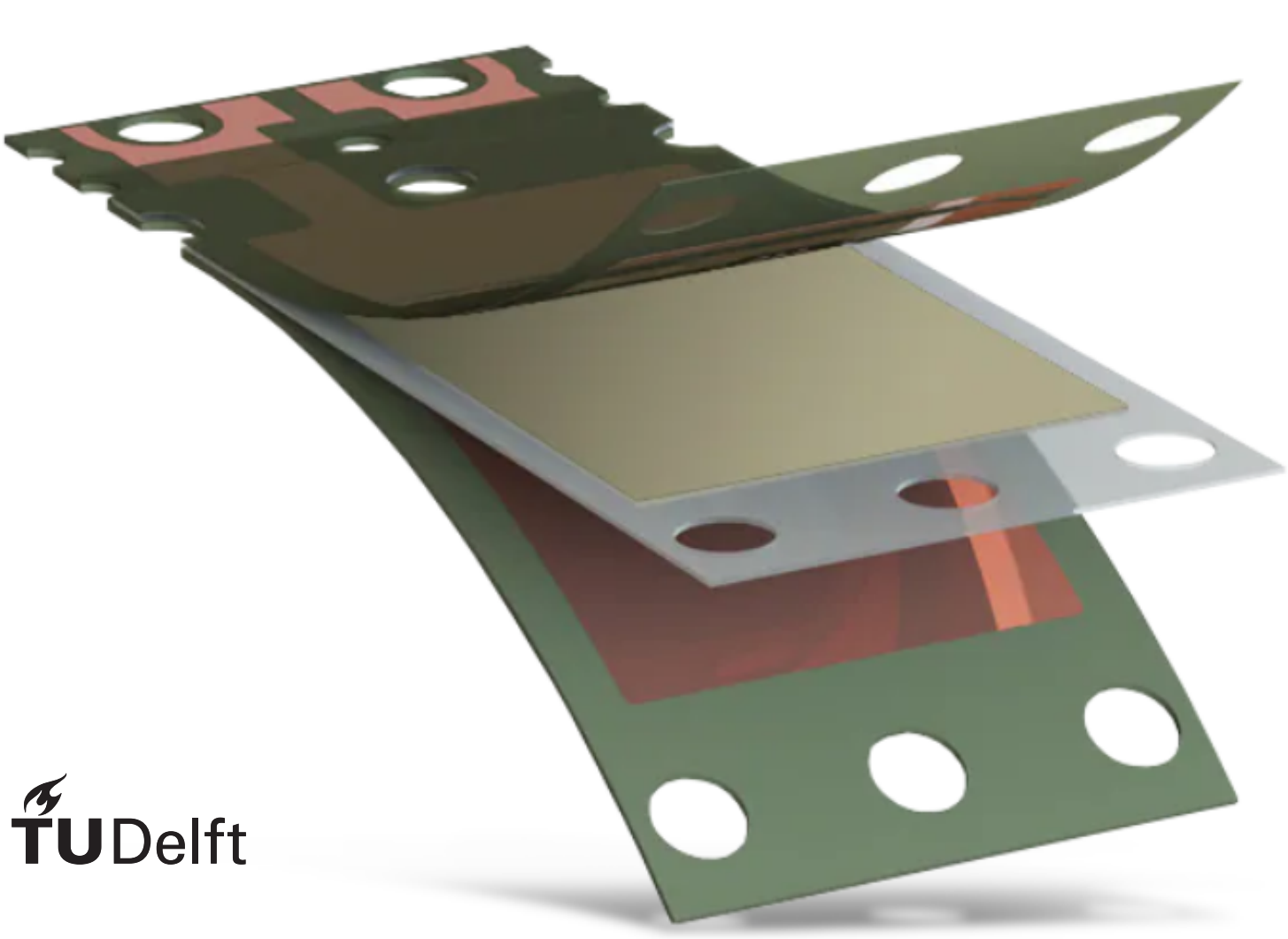

TU Delft

Piezoelectric Energy Harvesting System

for Low-Power IoT Sensors

by

Laurens-Jan Cammeraat
Wester Landman

to obtain the degree of Bachelor of Science
at the Delft University of Technology,
to be defended publicly on Friday June 27, 2025 at T.B.D. AM.

Student number:	Laurens-Jan Cammeraat	5144094
	Wester Landman	5640431
Supervisor:	Dr. Sijun Du	TU Delft
Project duration:	April 21, 2025 – June 27, 2025	

TU Delft

Abstract

Piezoelectric Energy Harvesting (PEH) offers a viable and sustainable solution for powering low-power electronic systems in hard-to-reach or maintenance-intensive environments, such as those found in aviation. The focus of this thesis lies on the circuit design aspect of the system, encompassing harvesting efficiency, regulation, and adaptive switching logic. The results validate that the proposed design fulfills the energy demands of a low-power wireless sensor, even under irregular excitation patterns.

A range of advanced rectifierless interface topologies are investigated, including Rectifierless Synchronous Electric Charge Extraction (ReL-SECE), Rectifierless Synchronized Switch Harvesting on Inductor (ReL-SSHI), and Parallel-SSHI (P-SSHI). These non-linear techniques are selected for their ability to maximize power output, eliminate diode thresholds, and dynamically adapt to varying load and vibration conditions, significantly improving power transfer compared to traditional full-bridge rectifiers.

Energy storage is realized through the use capacitors due to their rapid charge/discharge characteristics and long operational life. To ensure circuit safety and longevity, an over-voltage protection mechanism is implemented using a shunt regulator in combination with a resistive voltage divider. Additionally, a dedicated voltage regulation stage is incorporated to maintain a stable 3.3 V DC output, necessary for reliable operation of downstream wireless transmitters and onboard sensor systems.

The proposed system is designed to be energy-autonomous, capable of cold-start operation, and optimized for long-term deployment without the need for external maintenance or battery replacement. The approach aligns with current trends in micro-energy harvesting (MEH) for IoT applications, emphasizing compactness, adaptability, and robustness under real-world conditions. Overall, the system demonstrates the practical potential of intelligent, self-powered harvesting circuits in enabling sustainable sensor networks and instrumentation in modern aircraft environments.

Preface

This report is the result of our Bachelor graduation project for the Electrical Engineering program at TU Delft, completed over the course of ten weeks. Our project focused on the design and development of an efficient piezoelectric energy harvesting system capable of powering a low-power IoT sensor using ambient mechanical vibrations. The final system aims to enable long-term, maintenance-free operation of sensor nodes in environments where conventional power sources are not feasible, such as inside aircraft structures.

This project was carried out in collaboration with two other subgroups:

- **Subgroup 1 – Piezoelectric Transducer Characterization:** Ivo Sokal and Vincent Verkoren, who investigated the underlying working principles and behaviour of various piezoelectric materials under vibration.
- **Subgroup 3 – System Integration and Sensor Control:** Remon van Bemmel and Alessio Solter, who developed the microcontroller interface and implemented sensor measurements to validate the complete energy harvesting system.

We would like to express our sincere gratitude to our project supervisor, **Dr. Sijun Du**, for his guidance and technical insights throughout the project. We also thank our daily supervisors, **PhD Wenyu Peng** and **MSc Zijun Qiu**, for their continuous support, constructive feedback, and helpful discussions during design reviews and testing sessions.

Our goal is to give a thorough summary of our contributions and the technical choices we made during the project in this report.

Laurens-Jan Cammeraat
Wester Landman
Delft, June 2025

Contents

1 Introduction

The increasing adoption of Internet-of-Things (IoT) technologies in demanding environments such as aviation and industry has created a clear need for energy-autonomous sensors. These devices must be capable of operating for extended periods without the need for battery replacement or external power connections. In aircraft, where sensors may be embedded deep within structural components, accessing and maintaining them is both costly and impractical.[10] This drives the search for sustainable, maintenance-free power solutions.[6]

One promising approach is piezoelectric energy harvesting, which leverages the mechanical vibrations naturally present during aircraft operation to generate electrical energy. Piezoelectric materials convert mechanical strain into electrical charge, offering a compact and passive means of generating power.[8] However, the raw output from piezoelectric transducers is an irregular alternating current (AC) signal that cannot directly power typical electronics. To make this energy usable, it must be rectified, stored, and regulated into a stable direct current (DC) supply, capable of reliably powering low-power IoT sensors.

1.1. The goal of the project

This thesis is part of the Bachelor Graduation Project within the Electrical Engineering department at TU Delft, aimed at developing a piezoelectric energy harvesting system to power a low-power IoT sensor under realistic aircraft vibration conditions. Key challenges include efficient energy extraction from the transducer, AC-DC conversion with energy storage, and stable voltage regulation.

The project is carried out by six students divided into three subgroups. Subgroup 1 focuses on selecting and characterizing the piezoelectric transducer. The second subgroup, which is the focus of this thesis, is responsible for the design and implementation of the power conditioning circuit, tasked with converting and regulating the electrical output from the transducer. The third and final subgroup handles system integration, sensor interfacing, and testing.

1.2. Focus of This Thesis

This thesis focuses on the development of the power conditioning circuit for a piezoelectric energy harvesting (PEH) system, intended to power a low-power IoT sensor embedded within an aircraft structure. While the broader graduation project encompasses the complete system — including vibration characterization, transducer selection, and full-system integration — the scope of this thesis is specifically limited to the design, simulation, and practical implementation of the energy conversion and regulation stage.

The power conversion system serves as the critical interface between the piezoelectric transducer and the sensor load. The raw transducer output is typically an alternating, high-impedance signal with variable amplitude and frequency, unsuitable for direct use by electronic components. Therefore, a

dedicated power interface circuit is required to perform three essential functions: rectification of the AC signal, temporary energy storage, and regulation to a stable DC voltage output.

To meet these requirements, this work investigates a range of interface circuit topologies, starting from conventional full-bridge rectifiers and extending to advanced non-linear techniques such as SSHI (Synchronous Switch Harvesting on Inductor), SECE (Synchronous Electric Charge Extraction), and hybrid methods such as ReL-SSHI and ReL-SECE [1] [18]. These rectifierless or semi-passive approaches promise improved energy efficiency, especially under variable and low-amplitude vibration conditions, and reduced component count — important factors for embedded aerospace applications.

A key aspect of this thesis is to look at energy harvesting interface circuits under realistic vibration scenarios. The test platform was designed to allow controlled mechanical excitation (both sinusoidal and arbitrary waveforms), while simultaneously logging voltage and current across critical circuit points. The setup also supports a variety of load configurations, including purely resistive loads, capacitive elements, and supercapacitor-based storage. This structured approach ensures consistent, comparable performance assessments across different interface circuit topologies.

The final circuit selection was driven by a combination of simulation results and practical constraints, with particular attention paid to metrics such as harvested power, start-up voltage, cold-start behaviour, and long-term energy stability under fluctuating input conditions. By bridging theoretical analysis with experimental validation, this thesis contributes to a deeper understanding of PEH interface design for low-power embedded systems and offers insights into how different circuit topologies perform under real-world mechanical excitation.

1.3. Thesis Outline

The structure of this thesis follows a logical progression from background theory to the final experimental validation. Chapter 2, Background and Literature Review, presents the theoretical foundations of piezoelectric energy harvesting and reviews existing methods and techniques relevant to power conditioning systems. In Chapter 3, Program Requirements, the specific requirements for the energy harvesting system, including power management and system constraints, are outlined. Chapter 4, Design of the Proposed Circuit, describes the design process of the power conditioning circuit, focusing on the selection of appropriate topologies and their integration with the energy harvesting system. In Chapter 5, Simulation & Modelling, the simulation results are presented, demonstrating the predicted behaviour of the circuit under various conditions and mechanical inputs. Chapter 6, Experimental Results, details the experimental setup and presents the results of the hardware testing, comparing the performance of the designed circuit to the simulation predictions. Chapter 7, Conclusions, summarizes the findings, discusses the challenges encountered during the project, and provides suggestions for future improvements and work.

2

Background

2.1. PEH model

Piezoelectric materials are commonly used to harvest ambient mechanical energy. When subjected to vibration, they generate electrical charge through mechanical strain. The system can be modelled as a mechanical spring-mass system coupled to an electrical circuit via a transformer. At resonance, the piezoelectric device behaves like a sinusoidal current source in parallel with a capacitor and resistor as can be seen in figure 2.1 below[12].

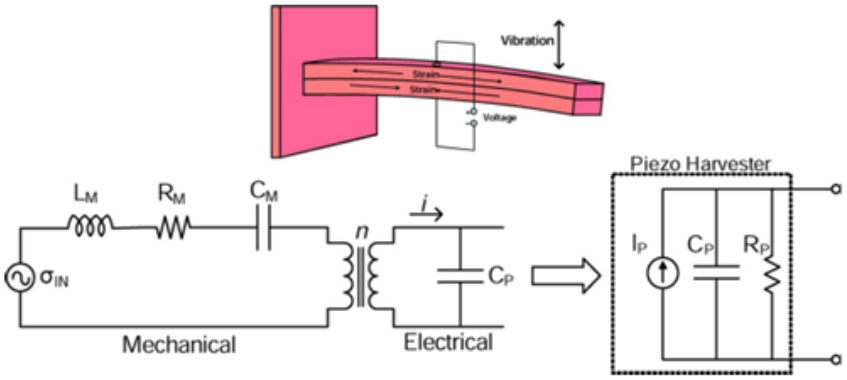

Figure 2.1: PEH equivalent circuit model[12].

2.2. Trends

In recent years, the design of power conditioning circuits for piezoelectric energy harvesters (PEH) has seen rapid development, driven by the increasing energy demands and miniaturization of IoT devices. As battery powered solutions prove impractical for large-scale or hard-to-reach deployments, research has shifted toward sustainable and autonomous energy systems - particularly micro energy harvesting (MEH) from ambient sources such as vibrations, solar radiation and thermal gradients[13].

A central trend in recent literature is the transition toward self-adaptive and self-configurable circuit architectures, which allow the harvesting system to respond dynamically to variable input conditions and load requirements. These systems aim to maximize power transfer by improving impedance matching, a critical factor in efficient energy harvesting. In addition, rectifierless topologies are increasingly replacing traditional diode rectifiers to reduce power loss caused by threshold voltages.

Techniques such as Synchronous Electric Charge Extraction (SECE) and Synchronous Switch Harvesting on Inductor (SSHI) have gained popularity due to their enhanced performance in minimizing

load dependency and improving integration at chip level. Capacitors are often used as passive reservoirs in these hybrid methods, enabling compact and efficient energy storage.

Further innovation is seen in multilevel energy extraction, bias-flipping, and multi-phase charge extraction, which collectively aim to minimize current dissipation in inductive components and reduce total circuit footprint. These strategies are particularly relevant for MEMS-scale PEHs, where space and energy efficiency are critical design constraints.

Looking ahead, the future of PEH and MEH technologies is expected to emphasize self-powered hybrid energy harvesting platforms. These systems will combine energy-aware power management, adaptive interfaces, and compact storage to support long-term, maintenance-free IoT operation. The evolution of these trends highlights a growing emphasis not only on energy conversion efficiency but also on the scalability and reliability of harvesting systems in real-world IoT environments [7].

2.3. Voltage regulation

In order to create a stable output voltage some kind of regulation stage is needed. Voltage regulation ensures that the electronic components especially sensitive low-power sensors receive safe and stable voltage. Without it, there is the possibility of incorrect operation or even permanent failure. Their are Two types of designs we can implement when for regulating the output, A linear regulator or a Switch mode supply.

A linear regulator controls the output voltage by continuously adjusting a resistive element between input and output. It drops the excess voltage as heat to keep the output steady. They are widely used for their simplicity, low cost, and ability to provide stable voltage output. They also generate very low noise and ripple which makes them them ideal for sensitive applications. They respond quickly to changes in load and require only a few external components making them easy to implement. Their major drawback is low efficiency, especially when the difference between input and output voltage is large the excess energy is dissipated as heat. This not only wastes power but also requires thermal management, making linear regulators less suitable for high power applications.

Switching regulators are much more efficient because they transfer energy using high-speed switching and energy storage elements like inductors and capacitors, which significantly reduces power loss. They are well-suited for applications that require stepping voltages up or down with minimal energy waste. Despite their efficiency and flexibility, switching regulators are more complex to design and typically generate more electrical noise and ripple due to their switching nature. They also require more external components and a careful PCB layout to control electromagnetic interference to not affect sensitive electronics[20].

3

Program of Requirements

The goal of this project is to design and implement a circuit that efficiently captures, stores, and distributes the electrical energy generated by the Piezoelectric Energy Harvester (PEH). This chapter outlines the various requirements that must be met in order to successfully achieve this objective.

3.1. Functional requirements

FR1 : The system shall include a storage component which collects the harvested energy.

FR2 : The system shall regulate the voltage to a usable level.

FR3 : The circuit shall be able to start from zero stored energy without external power.

FR4 : The system shall include components and control logic that enable continuous operation without the need for manual maintenance throughout the aircraft's service life.

FR5 : The system shall be able to generate and provide enough power to supply a sensor and a wireless transmitter.

3.2. System requirement

SR1 : The system shall make use of a bias flip rectifier.

SR2 : The circuit shall be able to operate within temperatures from -40 to 70 degrees Celsius.

SR3 : The system shall provide $3.3Volts$ of output voltage to the sensor and transmitter.

SR4 : The storage component shall be able to store enough energy to read out the sensor and transmit its data

SR5 : The harvesting system shall be able to draw more power from the PEH than a Full bridge rectifier.

SR6 : The entire system should lighter then $300grams$.

4

Design of the Proposed Circuit

Piezoelectric energy harvesting (PEH) converts mechanical vibrations into electrical energy. However, the raw signal from piezo elements is unsuitable for direct use or storage. To use this energy efficiently, a power management circuit is needed to rectify, condition, and store it. This chapter covers the design of the proposed system, consisting of three parts: the harvesting circuit, energy storage, and voltage regulation.

4.1. Harvesting circuit

There are various types of energy harvesting circuits available for implementation. For this project, we chose to simulate, build, and test four different topologies based on our research. These circuits were selected because they were both feasible to implement and showed potential to meet our design requirements. In this section, we explain the working principles of each of the four topologies and highlight their key strengths.

To design our circuit we use the equivalent circuit model in resonance from the literature review. A sinusoidal current source in parallel with a capacitor and a resistor. This model allows us to design a system that takes into account the high internal impedance of the piezoelectric generator, which limits the output current and voltage under ambient vibrations. This poses challenges for efficient rectifier circuit design.[12]

4.1.1. FBR

The Full Bridge Rectifier (FBR) is a widely used interface circuit that converts the alternating voltage generated by the PEH into DC. Its topology consists of four diodes arranged in a bridge configuration, as shown in Figure 4.1. During each half-cycle of the AC signal, two diodes conduct and allow current to flow in a single direction, producing a unipolar output.

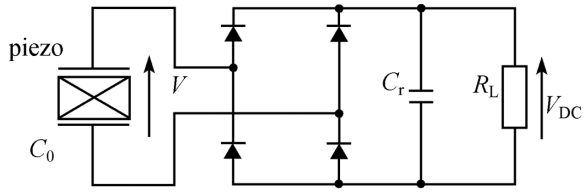

Figure 4.1: FBR circuit layout[11]

Although FBR is simple and easy to implement, it has notable drawbacks. Each conducting diode introduces a forward voltage drop (typically 0.6–0.7 V), resulting in significant energy loss. Furthermore, due to the phase mismatch between the piezoelectric voltage and current, especially at resonance, inefficient energy transfer occurs due to charge cancellation within the internal capacitance of the PEH

[19]. Although non-linear processing techniques can mitigate these effects, the FBR remains load-dependent and less efficient than advanced harvesting techniques.

Despite these limitations, the FBR serves as a baseline for the development of more advanced, non-linear interface circuits like SECE or SSHI.

4.1.2. ReL-SECE

The rectifier less Synchronous Electric Charge Extraction (ReL-SECE) method improves the efficiency of PEH by synchronizing the extraction of electrical charge with the voltage peaks induced by mechanical deformation. As the piezoelectric material undergoes strain, the charge accumulates until the voltage across reaches a maximum. At that point, the SECE interface extracts the stored charge through a synchronous switch that connects the element to an inductor and a storage capacitor, as shown in Figure 4.5. This results in a resonant energy transfer and inversely charging the piezoelectric voltage, optimizing the system for the next vibration cycle. It also eliminates the diode bridge, which typically introduces conduction losses[1].

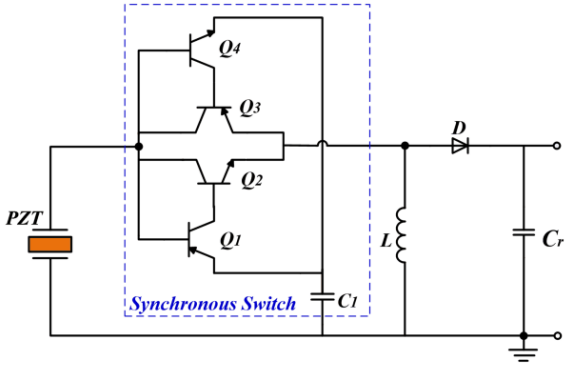

Figure 4.2: ReL-SECE circuit layout [1]

The circuit works in four stages. During the first stage were the PEH acts like a current source, naturally charges its internal capacitance. Voltage across the PEH increases until it reaches a peak. This peak is detected using a small capacitor C_1, which helps trigger the next stage.

In the second stage when the peak voltage is detected, the switch turns on. A part of the electric charge is extracted from Cp and transferred to the storage capacitor C_r through a diode. The remaining charge is inverted by creating an LC resonant loop between C_p and the inductor, negative charging the PEH.

The third stage is similar to step 1, but now the PZT generates a negative voltage due to the reversed mechanical input. Again, voltage builds to a negative peak, preparing for extraction and inversion. and this peak is also detected by the small capacitor of C_1.

and finally in the Fourth stage the negative voltage peak is detected and switch is triggered. the energy in the PEH is inverted via the LC loop now charging C_p with positive voltage. Then as the inductor discharges this energy is transferred to the storage capacitor C_r. This whole process can be seen in Figure 4.5.

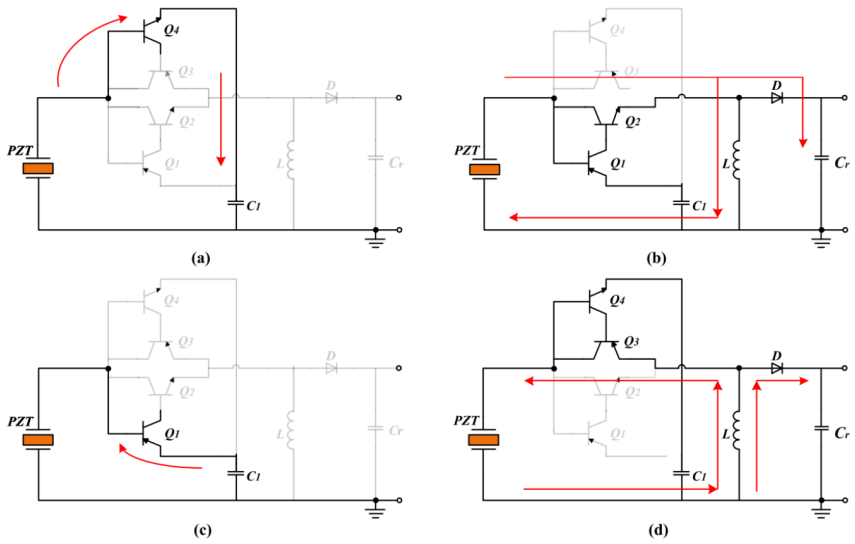

Figure 4.3: ReL-SECE working principle, (a) is stage one, (b) stage two, (c) stage three, (d) stage four. [1]

4.1.3. ReL-SSHI

The Rectifierless Synchronized Switch Harvesting on Inductor (ReL-SSHI) is a high efficiency non-linear technique that optimizes piezoelectric energy harvesting by replacing traditional diode-based rectification with controlled switch-based inversion [17]. Like Series-SSHI (S-SSHI), ReL-SSHI inverts the voltage across the piezoelectric element when the signal reaches its peak. However, it achieves this with significantly reduced losses due to the absence of diodes.

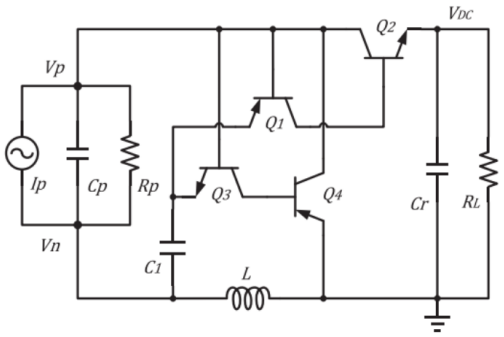

Figure 4.4: ReL-SSHI circuit layout [17]

As depicted in Figure 4.4, the ReL-SSHI circuit uses the transistors to selectively form LC resonance loops during the positive and negative voltage peaks, like the ReL-SECE discussed in section 4.1.3 the operation modes can be cut up into four district stages.

In the first stage the PZT generates current from environmental vibration.This current charges its internal capacitor C_p as well as a small capacitor C_1 used of peak detection. Voltage builds up across C_p until it reaches the positive peak.

At Stage two when the positive voltage peaks the transistors and create a resonant path with the piezoelectric capacitance C_p, the storage capacitor C_r, and the inductor L. Charging the storage capacitor C_r and inverting the voltage on C_p.

During stage three the PEH deforms now with reversed current direction, the current now negatively charges C_p and C_1. Voltage increases negatively until it reaches the negative peak.

In stage four at the negative peak, another LC loop is created to invert C_p back to a positive voltage. This is the biggest difference with the ReL-SECE discussed in because with the ReL-SSHI in stage four only the voltage on C_p is inverted, and no charge is directed to the storage capacitor C_r. The working of the four stages and the current flows can be seen Figure 4.5

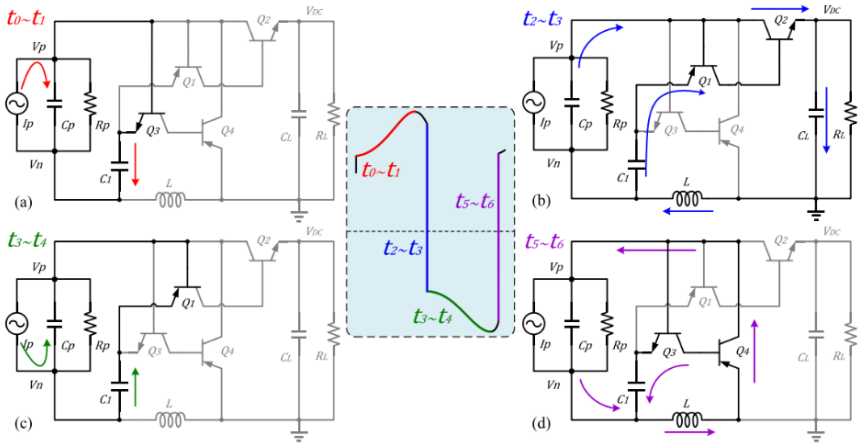

Figure 4.5: ReL-SSHI working principle, (a) is stage one, (b) stage two, (c) stage three, (d) stage four. [17]

Notably, ReL-SSHI can operate effectively even under low-voltage excitation conditions, unlike traditional S-SSHI circuits that suffer from diode threshold limitations. This makes ReL-SSHI highly suitable for low-energy environments and irregular vibration sources, as commonly encountered in wireless sensor networks and self-powered IoT applications[17].

4.1.4. P-SSHI

Parallel Synchronized Switch Harvesting on Inductor (P-SSHI) is a non-linear interface technique that increases energy harvesting by actively inverting the voltage across the piezoelectric device at key points in the vibration cycle [19]. The P-SSHI topology places the inductor and switch in parallel with the piezoelectric element, as illustrated in Figure 4.6.

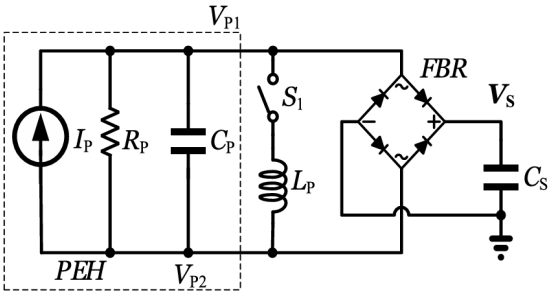

Figure 4.6: P-SSHI circuit layout [7]

At the voltage peak, the switch is momentarily closed. This forms a parallel LC resonance loop between the inductor and the piezoelectric capacitance. The resulting oscillation inverts the piezoelectric voltage. When the switch opens at the end of half a resonant cycle, the reversed voltage is preserved across the piezoelectric device, leading to a greater potential difference and enhanced energy transfer to the storage element through a rectifier.

The key advantage of the parallel configuration is its decoupling of the inversion resonance loop from the load, reducing energy losses associated with load impedance. This makes P-SSHI particularly efficient at higher excitation frequencies and in systems where load conditions fluctuate.
Successful implementation depends on precise peak detection and accurate timing of the switch activation to match half of the LC resonant period. Any deviation or excessive damping can result in incomplete voltage inversion and reduced efficiency. To create the switch the same topology of 4 transistors and a capacitor is used as for the synchronous switch used for the ReL-SECE discussed in 4.1.3.

4.2. Energy Storage in PEH Systems

4.2.1. Storage technique

In piezoelectric energy harvesting (PEH) systems, the generated electrical power is low and intermittent, especially under low-frequency or irregular vibrations. Since our application involves wireless sensing and data transmission, which require relatively high instantaneous power, an intermediate energy storage stage is necessary.

The harvested energy is commonly stored in either a capacitor or a rechargeable battery, each offering different advantages depending on the application context. Capacitors are well-suited for scenarios requiring rapid charge and discharge cycles. They exhibit a high power density, excellent cycle life, and can be charged quickly with low internal resistance. Batteries, by contrast, provide higher energy density and are more appropriate when sustained energy delivery over a longer time period is required [9].

In our design, energy is rectified and buffered in a storage element until a threshold voltage is reached. Once triggered, this energy is used to power components like sensors and RF transmitters. This buffer decouples the irregular nature of vibration energy from the deterministic needs of digital systems [9].

Capacitors offer fast charging, low internal resistance, and exceptional cycle life (10^5–10^6 cycles), making them ideal for applications with frequent, short energy bursts [14]. Batteries, on the other hand, provide significantly higher energy density (up to 265 Wh/kg) and are better suited for long-term energy storage in systems with infrequent vibrations [15]. However, while capacitors are more durable and charge quickly, they suffer from higher self-discharge rates. Batteries retain energy longer but degrade after $300 - -1000$ cycles and require slower, controlled charging to maintain stability [4].

As illustrated in Figure A.1, the choice between a capacitor and a battery depends on the application's specific power profile. Capacitors are well-suited for energy harvesting systems that require short bursts of high-power consumption, such as sensor activation and wireless transmission, due to their fast charging and high cycle life. This enhances system longevity and supports autonomous operation in remote or maintenance-limited environments. Meanwhile, hybrid storage systems that combine the high energy density of batteries with the fast response and durability of capacitors are gaining relevance, offering an effective balance between energy and power performance [5].

In this project, the choice of storage depends on the expected load profile. For our use case, with short bursts of high-power demand triggered by infrequent vibrations, capacitors are preferred due to their fast response and reliability. This approach supports robust, low-maintenance energy-autonomous operation.

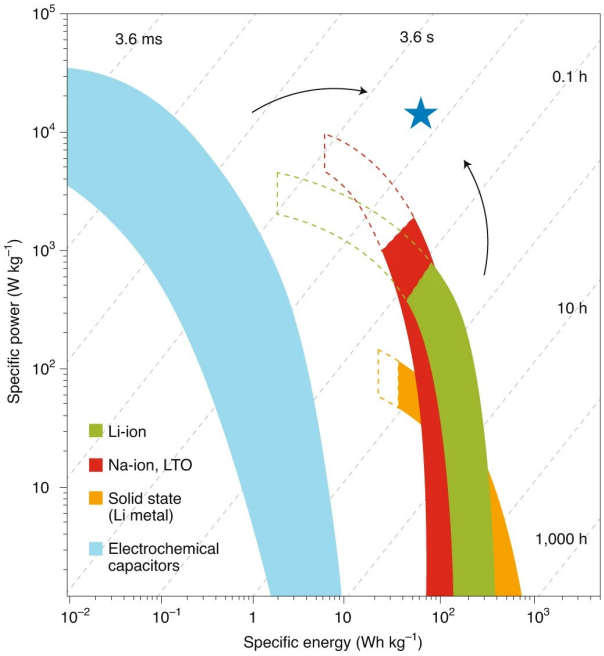

Figure 4.7: Comparison of energy storage technologies

4.2.2. Over-voltage protection

Since the energy stored in a capacitor is proportional to the square of the voltage, we need to protect our circuit from over-current caused by sudden, intense vibrations. These events could result in high voltage spikes across the capacitor, potentially damaging or destroying sensitive components.

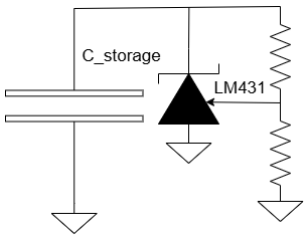

Figure 4.8: Capacitor Protection Design

To protect our circuit, we placed a shunt regulator and a resistive voltage divider in parallel with the storage capacitor. We are using the LM431 as the shunt regulator, which begins conducting when $2.5V$ is applied to its control pin. This control voltage is set using a pair of resistors forming a voltage divider, designed so that the control pin reaches $2.5V$ when the voltage across the capacitor rises to $6.5V$[16].

4.3. Voltage Regulation System

To ensure stable and reliable operation of the wireless sensor and transmitter, a regulated output voltage of $3.3V$ is required. Since fluctuations in supply voltage can lead to malfunction or instability of low-power electronics, a robust voltage regulation system is a critical part of the energy management design. The implemented regulation system consists of three main components: the regulator circuit, a switching mechanism, and a Schmitt trigger controller.

4.3.1. Regulator Circuit

The core of the voltage regulator is an op-amp-based feedback circuit that stabilizes the output voltage at $3.3V$. As shown in Figure 4.9, a diode generates a reference threshold voltage of approximately$0.5V$, which is applied to the non-inverting input of the op-amp. Meanwhile, a voltage divider at the inverting

input scales the output voltage down for comparison. The op-amp adjusts its output to ensure the inverting input matches the reference, thereby maintaining a stable $3.3V$ output.

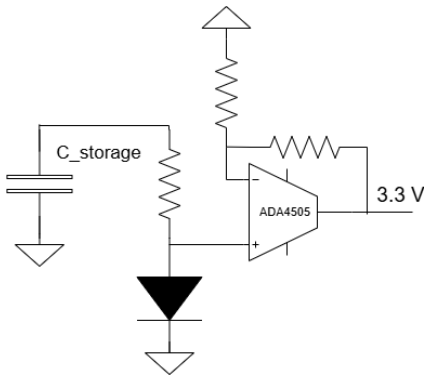

Figure 4.9: Voltage regulator based on op-amp with diode reference

While the capacitor is charging, this configuration draws only roughly $18uA$ of quiescent current as described in the datasheet [2]. This allows the capacitor to charge up to the desired energy level efficiently. However, once the switch closes and power is delivered to the load, the regulator behaves as a linear regulator. In this state, the voltage drop across the regulator ($V_{\text{cap}} - 3.3$ V) multiplied by the load current results in thermal dissipation, reducing efficiency during active power delivery.

4.3.2. Switching Control With Schmitt Trigger

To prevent premature power delivery, a switch is used to connect the regulated output to the load only when sufficient energy has been stored. This switching logic ensures that the system only powers up when the capacitor has charged to a voltage level high enough to support reliable operation [3].

Switching behaviour is controlled using a Schmitt trigger implemented with a second op-amp from the same dual op-amp IC. This circuit monitors the voltage across the storage capacitor and generates a clean digital control signal for the switch. As shown in Figure 4.10, the Schmitt trigger defines two distinct thresholds:

- When $V_{\text{cap}} > 5.5$ V, the output is high, closing the switch.
- When $V_{\text{cap}} < 2.8$ V, the output is low, opening the switch.

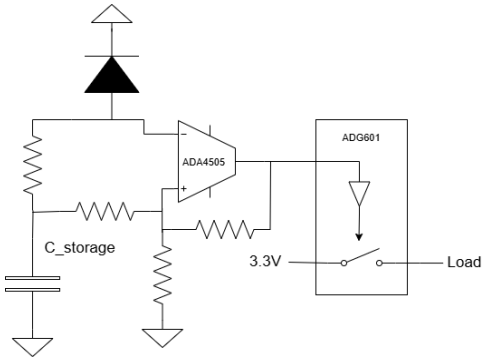

Figure 4.10: Schmitt trigger controlling the output switch

This hysteresis-based control prevents rapid toggling around a single threshold, which would otherwise result in unstable operation and energy loss. Replacing a traditional Zener diode with a Schmitt trigger significantly reduces static power consumption and provides more precise control, making this approach highly suitable for energy-constrained systems.

4.4. Overview

The entire system, shown below in Figure 4.11, can be divided into five distinct parts. First, a harvesting circuit is used to capture energy from the PEH and convert it into a DC voltage. The specific type of harvesting circuit will be determined in Chapter 6, where a comparative analysis of various energy harvesting techniques is presented.

The harvested energy is stored in a storage capacitor until it reaches a defined threshold. Connected to this capacitor is a voltage regulator that converts the capacitor voltage to a stable 3.3V, sufficient to power the sensor, transmitter, and associated components. Additionally, a Schmitt trigger is included to monitor the capacitor voltage and send a signal to the switch once the voltage is high enough.

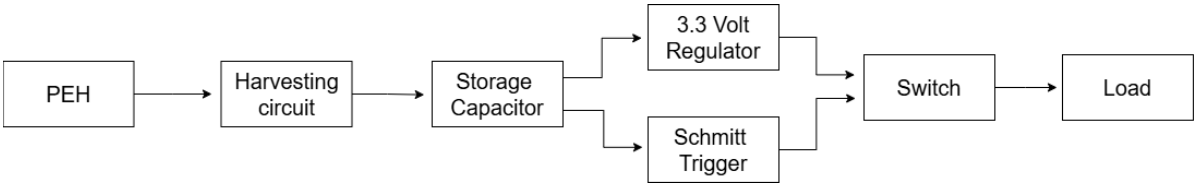

Figure 4.11: Block scheme of circuit

5

Simulation & Modelling

This section presents an analysis and comparison of several circuit topologies designed for piezoelectric energy harvesting. The investigated circuits include the Full Bridge Rectifier (FBR), Rectifierless Synchronized Electric Charge Extraction (ReL-SECE), Rectifierless Synchronized Switch Harvesting on Inductor (ReL-SSHI), and Parallel Synchronized Switch Harvesting on Inductor (P-SSHI). Simulations were carried out under identical input conditions to evaluate and benchmark the performance of each topology.

5.1. Simulation Harvesting circuits

All simulations were performed using LTspice. A sinusoidal current source was used to emulate the piezoelectric energy generator. An open-load configuration was selected to observe the natural charging behaviour of the storage capacitor without influence from a fixed resistive load. This approach allows us to evaluate how quickly the capacitor charges and to what voltage level. Which are key factors in determining when the microcontroller can be activated.

- Input frequency: $37Hz$
- Peak current: $38\ \mu$A
- Load resistance: open
- Piezoelectric capacitance: $22nF$

As shown in Figure 5.1, the results of multiple simulated circuits are displayed at the 5-second mark. Both the input voltage (Vin) and output voltage (Vout) are illustrated. It can be observed that the output voltage stabilizes into a DC-like signal, indicating successful energy conversion and regulation.

Table 5.1 summarizes the simulation results. It shows both the capacitor voltage after 5 seconds and the maximum open-circuit voltage. The power across a 500Ω load is also calculated to assess practical performance. The ReL-SECE circuit charges the fastest within the first 5 seconds, reaching a higher voltage earlier than the others. The focus on the 5-second mark was, ,because the key objective is to charge the storage capacitor as quickly as possible to activate the system and enable the microcontroller.

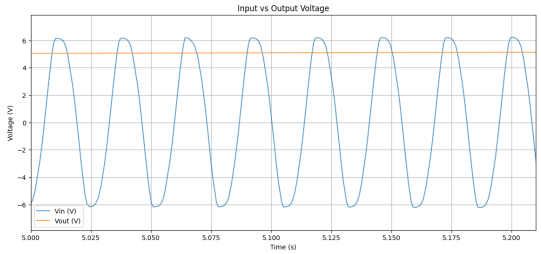

(a) FBR

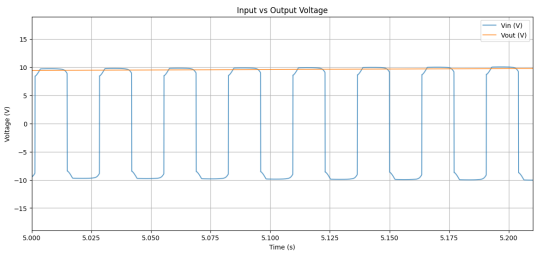

(b) P-SSHI

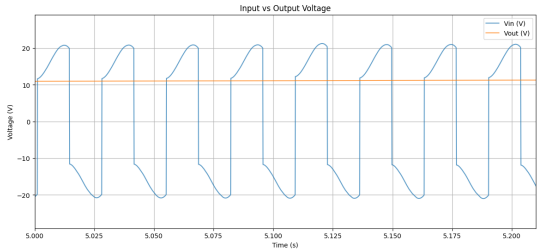

(c) ReL-SECE

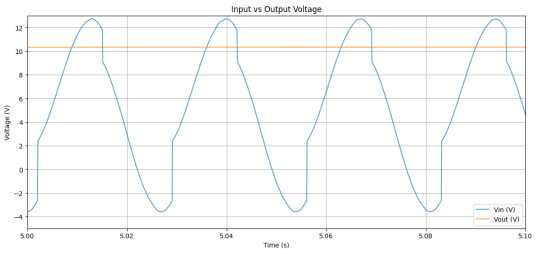

(d) ReL-SSHI

Figure 5.1: Overview of input vs output voltage for the four energy harvesting topologies

Table 5.1: Measured performance of different energy harvesting topologies

Topology	V_{out} after 5 sec (V)	V_{out} Open Max (V)	Power over 500 Ω (µW)
FBR	6.11	6.34	0.21
P-SSHI	9.40	41.36	0.27
ReL-SSHI	10.33	10.46	6.76
ReL-SECE	10.94	41.55	8.70

The open-circuit voltages for ReL-SECE and P-SSHI are also the highest, demonstrating strong energy harvesting capability under no-load conditions. Notably, while P-SSHI delivers high open-circuit voltage, its performance under load is more sensitive compared to ReL-SECE. P-SSHI relies heavily on optimal loading to maximize its benefit from charge inversion. In fact, with a 500 Ω load, the P-SSHI circuit behaves more like a conventional FBR, indicating that load matching is critical for achieving its full potential.

These results help identify ReL-SECE as a well-balanced performer for fast charging and high energy delivery, while P-SSHI shows strong potential in systems where the load conditions can be carefully controlled.

5.2. Regulation Circuit

The performance of the regulation stage depends on the voltage level of the storage capacitor. To model this behaviour in LTspice, we used a pulse voltage source, allowing us to accurately observe the circuit's response during both the charging and discharging phases of the capacitor. The voltage source is configured with a pulse waveform, starting at $0V$ and rising to $9V$, with rise time, on time, and fall time each set to 1 second.

5.2.1. Voltage regulator

The voltage regulator operates by allowing a small current to flow through a diode, generating a threshold voltage across it. This reference voltage is then amplified to produce a stable $3.3V$ output. The complete circuit, including all resistor values, is shown in the figures below.

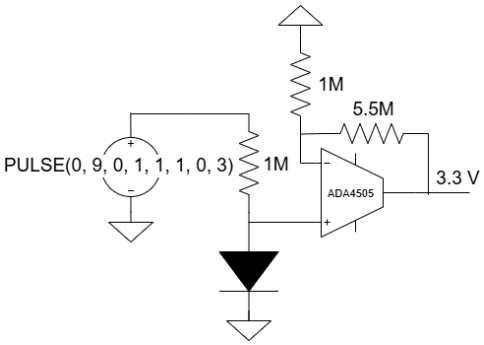

(a) 3.3V Regulator

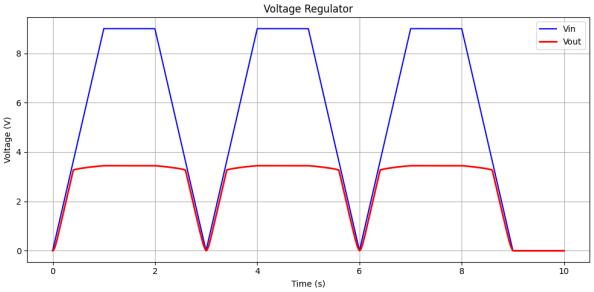

(b) Simulation results 3.3V regulator

Figure 5.2: Simulated regulator circuit and simulation results

It's clearly visible that the op-amp operates close to rail-to-rail output until the input voltage exceeds $3.3V$. From that point on, the op-amp begins to function as a linear regulator. As the input voltage continues to rise up to $9V$, the output slightly deviates from the target $3.3V$. This deviation is due to the threshold voltage set by the diode, which varies slightly with the current flowing through it. As the current changes, so does the diode's forward voltage, resulting in a small shift in the regulation threshold. A more detailed description of the working can be found in Section 4.3.1.

5.2.2. Schmitt trigger+Switch

The Schmitt trigger outputs a high signal when the voltage across the capacitor reaches $5.5V$, triggering the switch to connect the regulated $3.3V$ to the load. It also sets a lower threshold of $2.7V$, below which the $3.3V$ supply is disconnected from the load. The component values and corresponding voltage graph are shown below. A more detailed description of the working principle can be seen in section 4.3.2

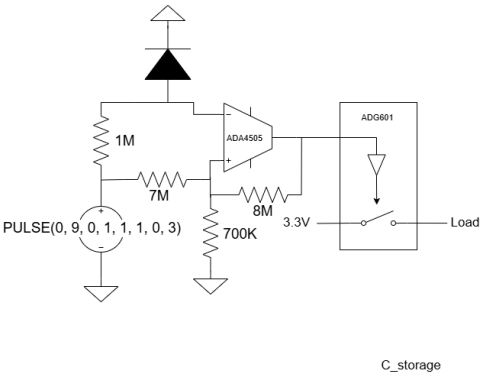

(a) Schmitt trigger + Switch

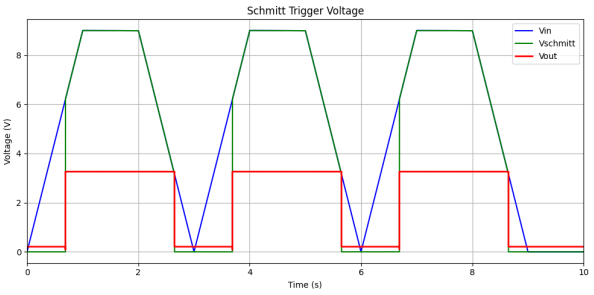

(b) Schmitt trigger + Switch simulation results

Figure 5.3: Simulated Schmitt trigger and switch results

5.3. Simulation Total Circuit

To evaluate the performance of the complete energy harvesting system, additional circuit blocks were included in the LTspice simulation: an energy storage capacitor, a control switch, and a voltage regulator. The goal of this setup is to ensure that a stable 3.3 V supply is available for powering a wireless sensor and microcontroller. Among the tested topologies, the P-SSHI circuit demonstrated the best performance, consistently delivering the highest output voltage and enabling efficient energy transfer to the storage stage.

The simulation uses the following conditions and component values:

- Storage capacitor: $1mF$
- Load Resistor: $500\ \Omega$
- Threshold voltage for activation: $5V$
- Lower voltage threshold: $3.3V$

As shown in Figure 5.4, the voltage across the storage capacitor gradually increases as energy is harvested and accumulated. Once the capacitor voltage reaches approximately $5V$, a switch is triggered, connecting the capacitor to a low-dropout voltage regulator. This regulator maintains a constant $3.3V$output as long as the capacitor voltage remains above the regulator's dropout threshold.

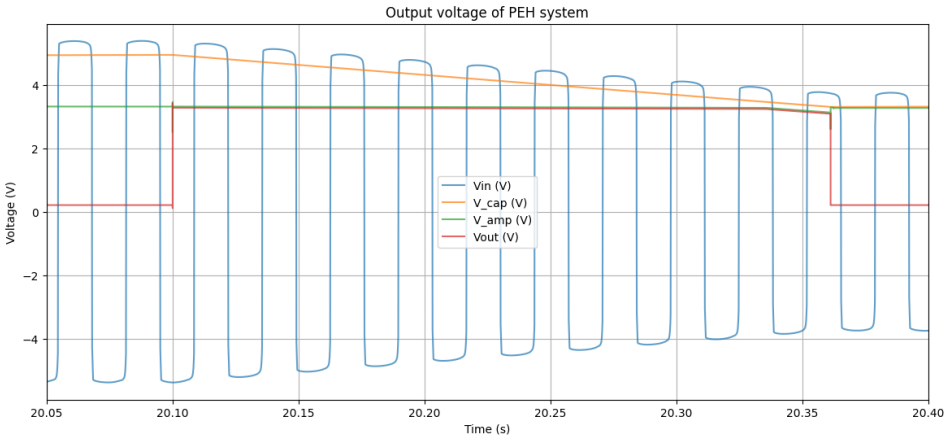

Figure 5.4: Simulation of PEH system

Eventually, the capacitor discharges to around $3.3V$, at which point the control logic disables the switch to prevent under voltage operation. The capacitor then begins recharging from the harvested energy, repeating the cycle. This burst-mode approach allows short but consistent periods of reliable operation, even under irregular mechanical excitation. In this setup, the controller has around $210ms$ to wake up, perform measurements, and transmit data. This simulation validates the system's ability to autonomously regulate power delivery, supporting intermittent but stable operation suitable for low-power embedded applications.

From the simulation, it is observed that the system initially requires approximately 20 seconds to charge the storage capacitor to the activation threshold of $5V$, marking the first point at which the regulator enables the $3.3V$ output. After this initial delay, the system operates in periodic bursts, with each cycle lasting around 8 seconds. During sleep mode, the microcontroller consumes minimal power, allowing the capacitor to recharge efficiently. In contrast, during active (wake-up) periods, the voltage on the capacitor drops more rapidly as energy is used for sensing and data transmission. Despite these fluctuations, the output voltage remains regulated and stable at $3.3V$ throughout operation. This confirms the system's capability to autonomously manage energy flow and maintain reliable performance, making it well-suited for intermittent, low-power wireless applications.

6

Implementation and Testing

This chapter presents the experimental results of the implemented piezoelectric energy harvesting circuits. All four topologies-FBR, ReL-SECE, ReL-SSHI, and P-SSHI-were tested using a piezoelectric element mounted on an electrodynamic shaker. The goal is to verify the behaviour of the designed circuits under actual mechanical excitation and to determine their suitability for powering ultra-low-power embedded systems.

To replicate the simulation conditions in a controlled environment, the piezoelectric harvester was mounted on a mechanical shaker driven by a signal generator at $58.2Hz$ with a 4.875 V_{pp} sine wave. The harvester, PPA-2011, was cantilevered with one end clamped, allowing optimal vibration response.

Tests were conducted using a 680 μF storage capacitor (plus 47 μF in parallel) and two reference capacitors ($2.2nF$ and $6.8nF$) to assess timing effects. Output performance was evaluated under open-load conditions, and with $50k\Omega$and $12.5k\Omega$ resistive loads to simulate real-world applications.

6.1. Circuit Performance Comparison

To evaluate and compare the performance of the four circuits, a series of measurements were conducted under different electrical load conditions. First, the output voltage was recorded across an open load, representing the theoretical maximum voltage the circuit could deliver. This gives insight into the peak energy harvesting potential without current draw. Additionally, the voltage was measured after 10 seconds of operation to assess the capacitor charging rate under no-load conditions.

In a more practical scenario, output voltages were also recorded while the circuit was connected to resistive loads of $50k\Omega$ and $12.5k\Omega$, simulating low- and high-power sensor applications respectively. Each measurement was repeated using two different reference capacitor values ($2.2nF$ and $6.8nF$), since the reference capacitance influences the resonant behaviour and switching dynamics in the SSHI-based topologies.

The results, summarized in Table 6.1, reveal that the P-SSHI circuit performs well across all measurement situations. It routinely outperforms the other topologies in terms of peak voltages, capacitor charging speed, and load performance. These experimental results validate previous modelling results and demonstrate P-SSHI's usefulness for efficient energy harvesting in low-power embedded devices.

Given its superior performance, the P-SSHI topology will be used entirely in the remaining tests and implementations detailed in this chapter.

Table 6.1: Measured Output Voltages for Each Topology under Various Conditions

Condition	FBR (V)	ReL-SECE (V)	ReL-SSHI (V)	P-SSHI (V)
Max voltage (2.2 nF)	4.2	3.8	6.3	**9.4**
Max voltage (6.8 nF)	N/A	4.3	6.2	**9.2**
Voltage after 10 s (2.2 nF)	2.1	1.5	1.9	**3.0**
Voltage after 10 s (6.8 nF)	N/A	1.7	2.1	**2.8**
Voltage over 50 kΩ (2.2 nF)	2.7	2.3	3.3	**4.9**
Voltage over 50 kΩ (6.8 nF)	N/A	2.3	3.3	**4.8**
Voltage over 12.5 kΩ (2.2 nF)	1.5	1.1	1.4	**2.1**
Voltage over 12.5 kΩ (6.8 nF)	N/A	1.2	1.5	**2.0**

6.2. Full System Testing

The performance of the entire energy harvesting system, including the voltage regulation and switching mechanism, was assessed by a series of practical experiments that used a function generator to replicate steady mechanical input. The experiment is aimed to determine the system's ability to maintain a consistent $3.3V$ output under various electrical loads and environmental disturbances, including introduced electrical noise. These tests shed light on the robustness and usefulness of the proposed harvester in real-world, low-power embedded applications.

6.2.1. Switching and Regulation Test

To assess the voltage regulation stage, the system was tested under various resistive loads to observe its ability to maintain a consistent output voltage.

Figure 6.1 shows the regulated output voltage across a $1M\ \Omega$ load. In this scenario, the storage capacitor successfully charged above the Schmitt trigger's upper threshold ($5.7V$), activating the switch and powering the regulator. The regulator maintained a stable $3.3V$ output for the duration of the test, validating the regulator's ability to provide clean, usable power to the load.

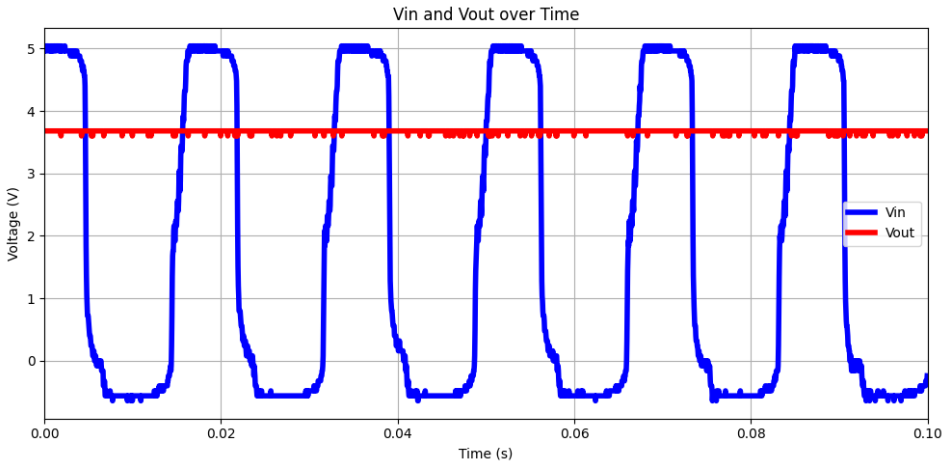

Figure 6.1: 1M □load 3.3 output voltage

A more dynamic scenario was tested using a $7k\Omega$ resistive load, as shown in Figure 6.7. With this lower load, the current draw exceeded the harvester's sustainable energy output. As a result, the system exhibited a cyclic charging and discharging behaviour: the capacitor charged to approximately $5.7V$, triggered the switch, and then rapidly discharged to $2.7V$ before the switch opened again. During the active phase, the regulator continued to provide a 3.3–$3.6V$ output. This behaviour confirms that the Schmitt trigger effectively manages power delivery in conditions of intermittent energy availability.

The system can maintain a regulated output of $3.3V$ for resistive loads as low as $11k\Omega$, according to the

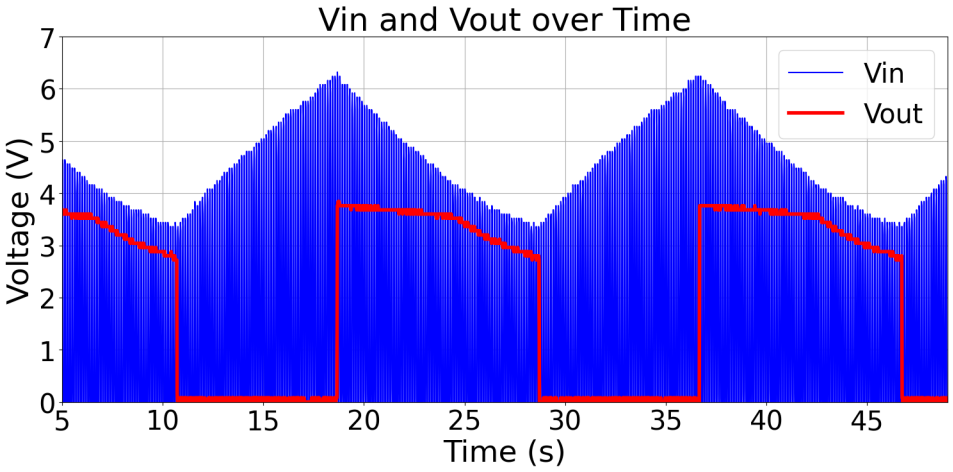

Figure 6.2: Voltage Output 7k

test results. Below this threshold, the system enters a pulsed mode of operation, in which the capacitor charges to the higher switching threshold, activates the load temporarily, and then disconnects as the voltage falls below the lower limit. Despite this irregular behaviour, the system continues to provide regulated power during each cycle. This indicates that the switching and regulating method is not only reliable, but also well-suited for ultra-low-power applications that require periodic operation.

6.2.2. Response To Noise Testing

To evaluate the robustness of the full energy harvesting system under real-world disturbances, the circuit was tested under three noise profiles, ranging from low to high interference levels. These profiles were created by adding controlled band-limited noise to a 58 Hz sine wave using a function generator. The exact Python implementation used to generate the noisy input signals is included in Appendix B.1.1.

Figure 6.3a shows the voltage behaviour at both the input and output under each noise condition, all tested using a 7 kΩ load. This load was selected to clearly visualize the operation of the system's Schmitt-trigger-controlled switch. During each cycle, the capacitor charges to approximately $5.6V$, after which the switch closes and the capacitor discharges down to $2.7V$. The output voltage remains regulated around $3.5V$ throughout this process.

The three levels of added noise amplitudes: 0.2, 0.6, and 0.8 demonstrate how increasing noise intensity affects system behaviour. At low noise levels (0.2), the system behaves similarly to a clean signal. The rise time of the capacitor remains approximately 16 seconds, comparable to the 15 seconds measured under ideal conditions. However, as noise increases, we observe the following effects:

The charging time to reach the switch threshold ($5.6V$) increases due to higher-frequency interference disturbing the harvester input. For example:

- Noise low: ∼16 seconds
- Noise medium: ∼23 seconds
- Noise high: ∼28 seconds

The initial voltage drop after the switch closes becomes sharper with more noise. With no or low noise, the discharge of the capacitor is smooth and gradual. However, under higher noise levels, the first drop in V_{cap} immediately after switching is significantly steeper—likely due to noise-induced fluctuations in the internal resistance and energy path stability.

In addition to timing, the system's ability to maintain a continuous regulated output is also affected by noise. The minimum sustainable load the smallest resistance for which regulation remains stable without reverting to pulsed operation increases with noise level:

- **Noise low:** stable down to $15k\Omega$
- **Noise medium:** stable down to $20k\Omega$
- **Noise high:** stable down to $25k\Omega$

These results confirm that the energy harvester and its control logic remain functional across all tested conditions. While higher noise increases charging time and reduces the system's tolerance to heavier loads, regulation continues successfully. This demonstrates that the design is suitable for ultra-low-power applications even in electrically noisy or unstable environments

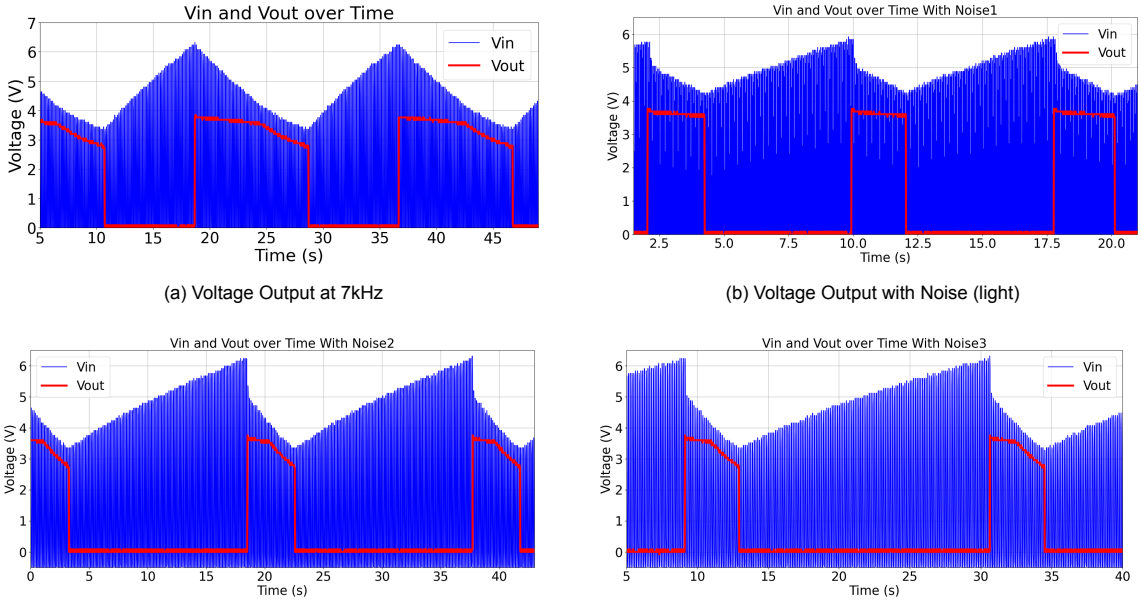

(a) Voltage Output at 7kHz

(b) Voltage Output with Noise (light)

(c) Voltage Output with Noise (medium)

(d) Voltage Output with Noise (heavy)

Figure 6.3: Voltage outputs under various noise levels and operating conditions.

6.2.3. Power Consumption with integration of sensor

To evaluate the power consumption and system behaviour under realistic sensor activity, two transmission strategies were investigated: single-packet transmission and burst-mode transmission. In the first case, illustrated in Figure 6.4a, a single data packet is transmitted once the storage capacitor reaches the switching threshold. The system regulates the output voltage to 3.3 V and successfully completes the transmission without any instability, demonstrating reliable performance under low-duty-cycle operation.

In the second scenario, shown in Figure 6.4b, the system attempts burst transmission, sending three to five sensor readings in rapid succession during one discharge cycle. This results in a sharp initial voltage drop followed by a gradual decline as the capacitor discharges. Toward the end of the burst, a small amount of voltage jitter is observed, caused by diminishing voltage headroom during the final pulses. Despite this, all transmissions complete successfully, demonstrating the system's resilience under high instantaneous current draw.

However, one limitation arises when using analogue sensors. Since their output is directly influenced by the supply voltage, the observed jitter and voltage fluctuations near the end of a burst may introduce measurement inaccuracies. This highlights a potential trade-off between transmission strategy and sensing accuracy. For future iterations, using digital sensors or incorporating an internal voltage reference may help mitigate these effects.

To verify the adequacy of the energy storage, updated measurements were taken under realistic transmission conditions. A single sensor transmission consumes approximately 5.37 mJ, based on a current

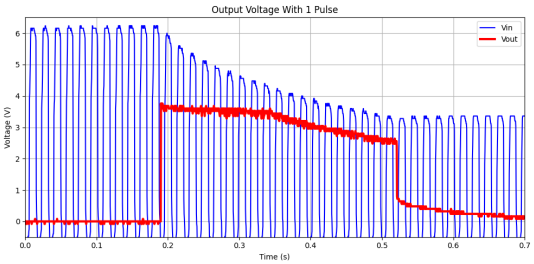

(a) Output Voltage With 1 Pulse

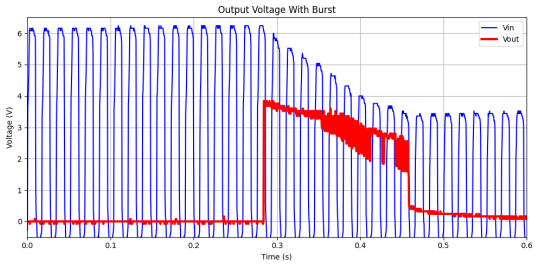

(b) /Output Voltage With Burst

draw of 4.9 mA over 332 ms at 3.3 V. In burst mode, where three to five packets are sent consecutively, the system draws around 12 mA for 176 ms, totaling roughly 6.97 mJ. These values align closely with the energy stored in the 680 μF capacitor at full charge, confirming the storage design is sufficient for both modes of operation. Full calculations are provided in Appendix A.4.

These results demonstrate that the system reliably supports both low-duty-cycle and high-throughput transmission modes. Even under burst conditions, the power management circuitry maintains voltage regulation and ensures sufficient energy delivery. This confirms the effectiveness of the overall design in enabling stable, autonomous wireless sensing from harvested energy.

6.2.4. Storage capacitor size

The size of the storage capacitor significantly impacts the system's performance. A larger capacitor allows the load to be powered for a longer duration, enabling more data to be transmitted within a single cycle. However, the trade-off is a longer charging time. To find the optimal balance, we tested the complete system with various capacitor sizes to determine the most suitable option, the results of which can be seen below in figure 6.5.

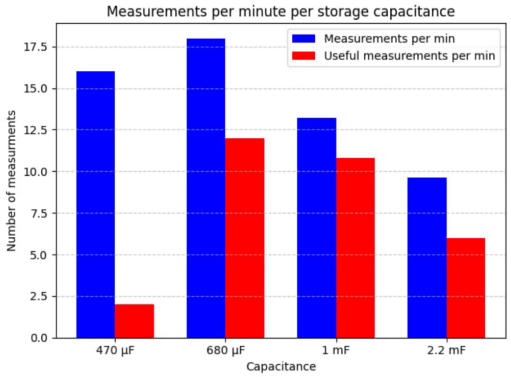

Figure 6.5: data rate

From our tests, we observed that with the 470μF capacitor, data could be transmitted very frequently. However, the supplied voltage began to deviate quickly, resulting in most of the transmitted data being incorrect. Using a 680μF capacitor, we noted a slight increase in the amount of data sent, along with a significant improvement in data accuracy. With a $1mF$ capacitor, nearly all transmitted data was correct, but the longer charging time reduced the overall transmission frequency. As a result, despite the high accuracy, the total volume of correct data per minute was lower. The $2.2mF$ capacitor appeared to have substantial internal leakage. It required a very long time to charge, and while it was able to transmit a large dataset once fully charged, the number of useful measurements per minute was relatively low. Based on these results, we selected the 680μF capacitor for energy storage, as it provided not only the highest number of measurements per minute but also the greatest number of useful measurements over time.

6.3. Regulation efficiency

To evaluate the power consumption and efficiency of the regulation stage, we used a DC power supply and a 470Ω load to emulate the behaviour of the storage capacitor and sensor load. This setup allowed us to increment the supply voltage in $0.1V$ steps and take precise current measurements.

6.3.1. Discharging

The results below show the current drawn by the system while the load is connected and the capacitor is discharging. We can clearly observe that when V_S is above $4.5V$, a significant portion of the current is wasted in other parts of the circuit, leading to considerable inefficiency during the initial phase of the discharge cycle. However, when the capacitor voltage drops to between $4.5V$ and $3.6V$ the circuit executes the desired behaviour, nearly all of the drawn current flows to the load, and the system operates with approximately 80 percent power efficiency.

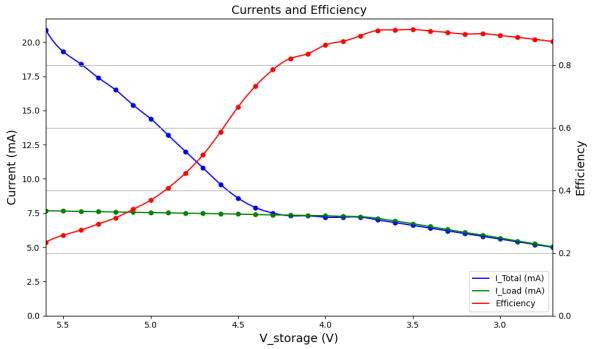

Figure 6.6: Current drawn and power efficiency

6.3.2. Charging

Even when the load is switched off, a small amount of current continues to flow into the regulation circuit. This quiescent current is largely due to the ADA4505-2 op-amp, which, according to the datasheet, draws approximately 15μA [2]. Additionally, small currents flow through various resistors and a diode that are necessary for correct circuit operation. The graph below shows the system's quiescent current during the charging phase. It can be clearly seen that the quiescent current stabilizes at around 27μA

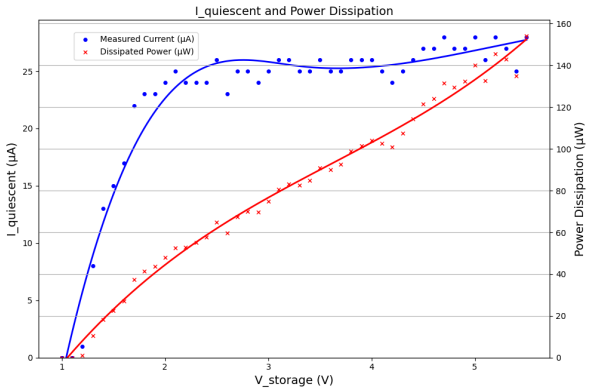

Figure 6.7: Quiescent current end power draw during charging

quickly during the charging phase. When the voltage across the storage capacitor reaches $5.6V$. At this point, approximately 150μW of power is dissipated.

7

Discussion

Although the system functions correctly in most cases, some unwanted behaviours in the circuit reduce its overall efficiency. A likely cause of these issues is the use of breadboards for most of the assembly, which introduced unreliable connections and potential contact faults. In this chapter, we will explain these behaviours in detail and present small fixes that could be implemented to address them.

7.1. Regulator topology

In section 6.3.3 figure b we can see that when the load is operating in burst mode, a large dips in supply voltage occur due to the sudden draw of large currents. This is because the Op-Amp is not able to supply these currents on it own, therefore we suppose to use a second storage capacitor at the output of the regulator to deal with these sudden high current demands.

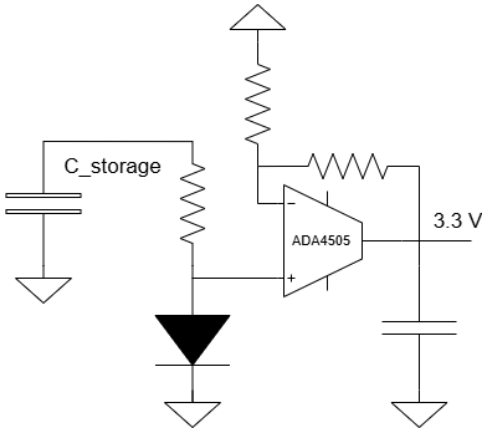

Figure 7.1: Comparison of energy storage technologies

7.2. Schmitt trigger

In our current system, the switch turns on when the voltage across V_S reaches $5.6V$ and turns off when it drops to around $2.7V$. This hysteresis effect allows the capacitor to charge and discharge effectively, enabling stable operation. However, as shown in Figure 6.6, at voltages above $4.3V$, a significant amount of energy is wasted in various parts of the circuit. Additionally, when falls below $3.3V$, the sensor's supply voltage becomes too low to produce reliable data.

By adjusting the control resistor values so that the system switches on at $4.3V$ and off at $3.3V$, we can significantly reduce the charging time. This would allow the system to transmit more data per minute and operate more effectively under lower excitation levels, since the required voltage is substantially reduced.

8

Conclusions

The objective of this project was to establish a completely self-sufficient energy harvesting system that could use a piezoelectric transducer to power a wireless sensor node. This requires that the system function without an external power source and to require no maintenance throughout the operational life. In addition, it had to maintain stable performance across varying environmental conditions, including noisy or inconsistent inputs. The foundation of the design and validation process was created by converting these design objectives into specific functional and system-level requirements.

Throughout the development process, each core functional requirement was addressed and successfully validated. The system was shown to be capable of cold-starting without any pre-stored energy (FR3), maintaining a stable output voltage of $3.3V$ (FR2, SR3), and storing harvested energy in a dedicated storage module (FR1). Importantly, it was able to continuously operate without the need for external maintenance (FR4), and it provided enough energy to support both sensing and wireless transmission tasks (FR5). These outcomes confirm not only the technical feasibility of the concept, but also its potential relevance in practical aerospace deployments.

At the system level, several key design choices contributed to the circuit's strong performance. A bias-flip rectifier was implemented in place of a traditional full-bridge design (SR1), significantly improving conversion efficiency. All components were carefully selected to ensure reliable operation across the required temperature range from $-40°C$ to $70°C$ (SR2), and the energy storage system was dimensioned to support realistic duty cycles of sensing and data transmission (SR4). The complete solution was realized in a compact, lightweight form factor (SR6), reinforcing its suitability for integration in space-constrained aerospace environments.

The energy harvesting topology was a significant consideration. After considering various options, a Parallel Synchronous Switch Harvesting on Inductor (P-SSHI) setup was chosen. The decision was backed by theoretical models and later confirmed through practical experimentation. The P-SSHI circuit consistently demonstrated higher energy extraction efficiency, better voltage stability, and greater resilience to electrical disturbances compared to more conventional designs. This choice was instrumental in satisfying the requirement for maximized energy harvesting (SR5).
Overall, this thesis demonstrates that an energy-autonomous system based on piezoelectric harvesting can reliably power wireless sensor nodes under noisy conditions. The P-SSHI topology was validated both in simulation and in practice, outperforming conventional approaches in energy efficiency and voltage stability. Through careful system design, including cold start capability, effective voltage regulation, and adaptive switching. The design meets all functional and system-level requirements, confirming its suitability for future aerospace integration.

9

Future Work

In this project, we made significant progress toward integrating the PEH, enabling both energy extraction and wireless data transmission. However, since the project was conducted over a limited period of just 10 weeks, there are still several steps and improvements that we have not yet explored or implemented. In this chapter, we discuss potential next steps and examine how they could impact system performance and contribute to the development of a fully functional product.

9.1. Integration on PCB

For any electronic circuit to be viable for commercial distribution, it must be integrated onto a printed circuit board (PCB). We designed the PCB layout for our circuit using KiCad 9 and have already placed an order for it. However, at the time of writing the board has not yet arrived. A 3D rendering of the PCB is shown in the figure 9.1.

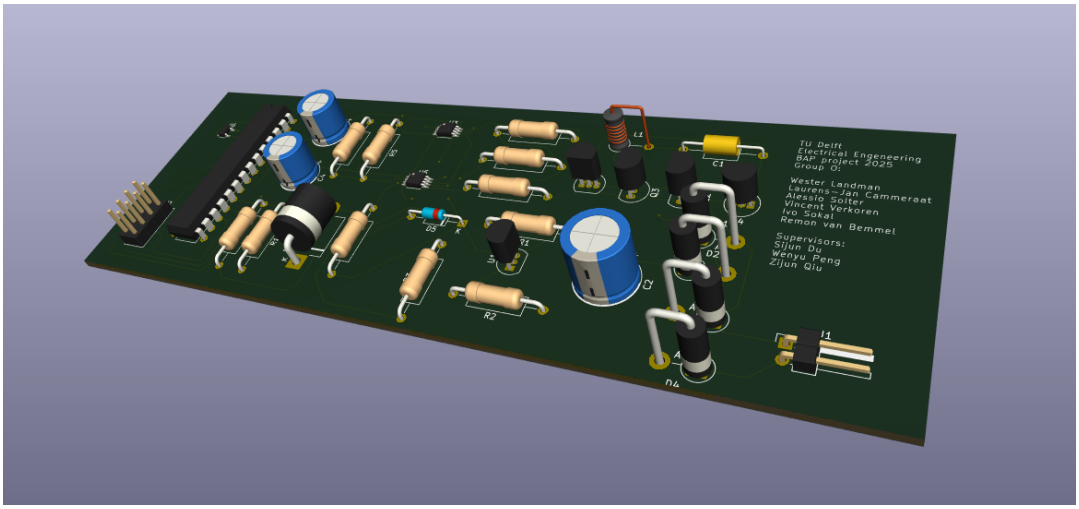

Figure 9.1: 3D rendering of PCB

This is still a prototype consisting of mostly through-hole components to make it easy to swap them out when adjusting values. However for a finalized product the goal would be to design a PCB using primarily surface-mounted (SMD) components, in order to create a system that is as compact and lightweight as possible.

9.2. Rectifier less Harvesting techniques

In our design, we used a P-SSHI (Parallel Synchronized Switch Harvesting on Inductor) extraction circuit to maximize the voltage across the PEH and efficiently convert it using a full-bridge rectifier. While the full-bridge rectifier introduces some losses due to the threshold voltage of the diodes, we found it to be the most effective option.

Although we researched, built, and tested rectifierless designs, they proved to be less efficient than the P-SSHI configuration in our setup. However, we believe there is still significant potential in rectifierless energy harvesting techniques, and that further research and testing could lead to even more efficient solutions.

9.3. Switching regulators

Switching regulators offer the potential for higher efficiency during operation compared to our current design, which uses an op-amp functioning as a linear voltage regulator. In our approach, the capacitor voltage is converted to $3.3V$ when connected to the load, with the excess voltage being dissipated as heat. While this results in some power loss, the system we developed is highly efficient when the switch is closed and also supports cold start capability. Nevertheless, investing effort into designing a switching-type regulator could lead to improved overall efficiency.

Bibliography

[1] Zhidong Chen et al. “A Novel Rectifier-Less Synchronous Electric Charge Extraction and Inversion Interface Circuit for PE Energy Harvesters”. In: *IEEE Transactions on Power Electronics* 39.3 (Mar. 2024), pp. 3749–3760. DOI: 10.1109/TPEL.2023.3346872.

[2] Analog Devices. *ADA4505-1/ADA4505-2/ADA4505-4 Data Sheet*. Tech. rep. 2017. URL: https://www.analog.com/media/en/technical-documentation/data-sheets/ADA4505-1_4505-2_4505-4.pdf.

[3] Analog Devices. *Data Sheet ADG601/ADG602*. Tech. rep. 2025. URL: https://www.analog.com/media/en/technical-documentation/data-sheets/ADG601_602.pdf?ADICID=SYND_WW_P682800_PF-spglobal.

[4] D. Dondi et al. “Battery-less wireless sensor node powered with ultra-low power energy harvesting”. In: *Microelectronics Journal* 39.12 (2008), pp. 1469–1476. DOI: 10.1016/j.mejo.2008.01.012. URL: https://doi.org/10.1016/j.mejo.2008.01.012.

[5] Claire Dupas, Patrice Simon, and Yury Gogotsi. “Trends in Electrochemical Capacitor and Battery Technologies”. In: *Nature Materials* 19 (2020), pp. 999–1005. DOI: 10.1038/s41563-020-0747-z. URL: https://www.nature.com/articles/s41563-020-0747-z.

[6] “Energy harvesting techniques for wireless sensor networks: A systematic literature review”. In: 57 (Jan. 2025). ISSN: 2211467X. DOI: 10.1016/j.esr.2024.101617. URL: https://linkinghub.elsevier.com/retrieve/pii/S2211467X24003262.

[7] Sima Ghandi, Mohammad Al Janaideh, and Lihong Zhang. *State of the Art on Power Conditioning for Piezoelectric Energy Harvesters*. 3. Feb. 2024. URL: https://doi.org/10.1109/TPEL.2023.3345663.

[8] Iman Izadgoshasb. “Piezoelectric Energy Harvesting towards Self-Powered Internet of Things (IoT) Sensors in Smart Cities”. In: *Sensors* 21.24 (Dec. 2021), p. 8332. DOI: 10.3390/s21248332. URL: https://doi.org/10.3390/s21248332.

[9] Ch Naveen Kumar. “Energy collection via Piezoelectricity”. In: *Journal of Physics: Conference Series*. Vol. 662. 1. International Conference on Vibration Problems (ICOVP-2015). IOP Publishing, 2015, p. 012031. DOI: 10.1088/1742-6596/662/1/012031. URL: https://doi.org/10.1088/1742-6596/662/1/012031.

[10] M. R. Pearson et al. *Energy Harvesting for Aerospace Structural Health Monitoring Systems*. Conference Report. Presented at Modern Practice in Stress and Vibration Analysis 2012 (MPSVA 2012); published in *Journal of Physics: Conference Series*, Vol. 382, 012025. DOI: 10.1088/1742-6596/382/1/012025. Queen’s Buildings, The Parade, Newport Road, Cardiff, CF24 3AA, United Kingdom: Cardiff School of Engineering, Cardiff University, 2012.

[11] Jinhao Qiu et al. “Comparison between Four Piezoelectric Energy Harvesting Circuits”. In: *Frontiers of Mechanical Engineering in China* 4.2 (2009), pp. 153–159. DOI: 10.1007/s11465-009-0031-z. URL: https://doi.org/10.1007/s11465-009-0031-z.

[12] Yogesh K. Ramadass and Anantha P. Chandrakasan. “An efficient piezoelectric energy harvesting interface circuit using a Bias-Flip rectifier and shared inductor”. In: *IEEE Journal of Solid-State Circuits* 45.1 (Jan. 1, 2010), pp. 189–204. DOI: 10.1109/jssc.2009.2034442. URL: https://doi.org/10.1109/jssc.2009.2034442.

[13] Mahidur Sarker et al. “Micro energy harvesting for IoT platform: Review analysis toward future research opportunities”. In: *Heliyon* 10.6 (2024), e27778. DOI: 10.1016/j.heliyon.2024.e27778.

[14] P. Simon and Y. Gogotsi. “Materials for electrochemical capacitors”. In: *Nature Materials* 7.11 (2008), pp. 845–854. DOI: 10.1038/nmat2297. URL: https://doi.org/10.1038/nmat2297.

[15] J.-M. Tarascon and M. Armand. “Issues and challenges facing rechargeable lithium batteries”. In: *Nature* 414.6861 (2001), pp. 359–367. DOI: 10.1038/35104644. URL: https://doi.org/10.1038/35104644.

[16] Texas Instruments Incorporated. *HDC1080 Low Power, High Accuracy Digital Humidity Sensor with Temperature Sensor*. Jan. 2016. URL: https://www.ti.com/lit/ds/symlink/hdc1080.pdf?ts=1732983821201&ref_url=https%253A%252F%252Fwww.ti.com%252Fproduct%252FHDC1080%253Futm_source%253Dgoogle%2526utm_medium%253Dcpc%2526utm_campaign%253Dasc-null-null-gpn_en-cpc-pf-google-wwe%2526utm_content%253Dhdc1080%2526ds_k%253DHDC1080+Datasheet%2526dcm%253Dyes%2526gad_source%253D1%2526gclid%253DCjwKCAiAjKu6BhAMEiwAx4UsApc-Qpjuz0-QdKoqiPqylv5m6AX-HbGpM-5zFII82OCtfdHzUKrngxoChLYQAvD_BwE%2526gclsrc%253Daw.ds.

[17] Xiudeng Wang et al. “A Self-Powered Rectifier-Less Synchronized Switch Harvesting on Inductor Interface Circuit for Piezoelectric Energy Harvesting”. In: *IEEE Transactions on Power Electronics* 36.8 (Aug. 2021), pp. 9149–9160. DOI: 10.1109/TPEL.2021.3052573.

[18] Huakang Xia et al. “A self-powered PSSHI and SECE hybrid rectifier for piezoelectric energy harvesting”. In: *IEICE Electronics Express* 17.17 (2020), pp. 1–5. DOI: 10.1587/elex.17.20200269. URL: https://doi.org/10.1587/elex.17.20200269.

[19] Yi Yang et al. “Circuit Techniques for High Efficiency Piezoelectric Energy Harvesting”. In: *Micromachines* 13.7 (2022). This article is an open access article distributed under the terms and conditions of the Creative Commons Attribution (CC BY) license., p. 1044. DOI: 10.3390/mi13071044. URL: https://doi.org/10.3390/mi13071044.

[20] Henry J. Zhang. “LINEAR REGULATORS”. In: *Application Note 140* (Sept. 2013). URL: https://www.analog.com/media/en/technical-documentation/app-notes/an140.pdf.

A

A.1. Circuit Design LTspice

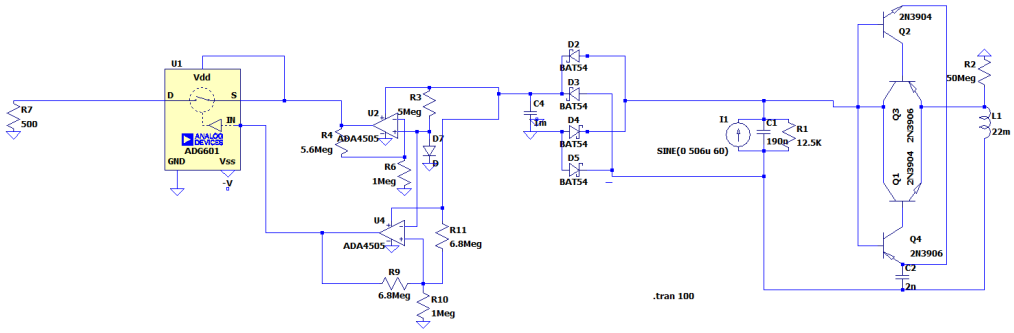

Figure A.1: Circuit design Toplogy

A.2. Extra Waveforms

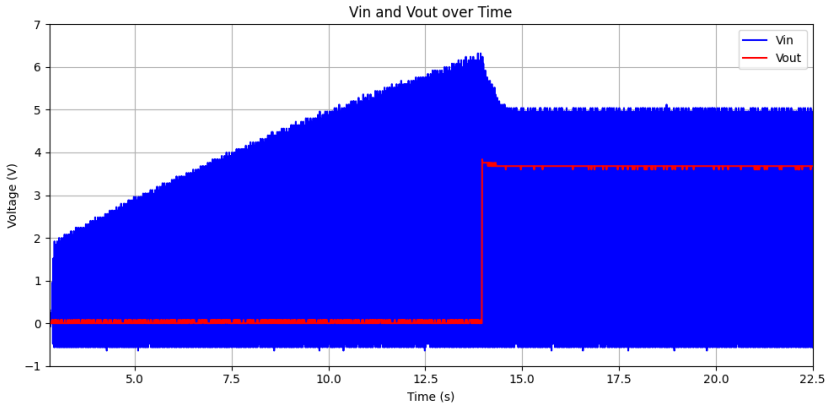

Figure A.2: Vin Vout intial TIme

A.3. Setup Experiment

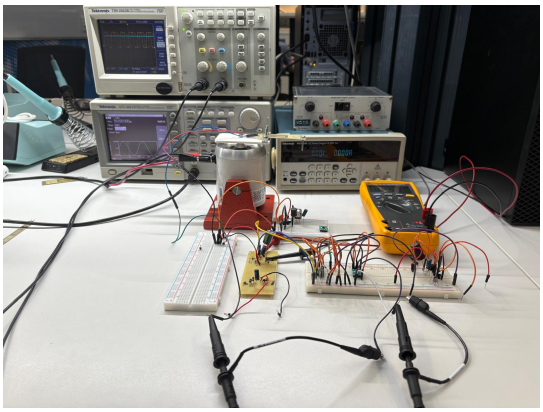

(a) Setup of Experiment 1

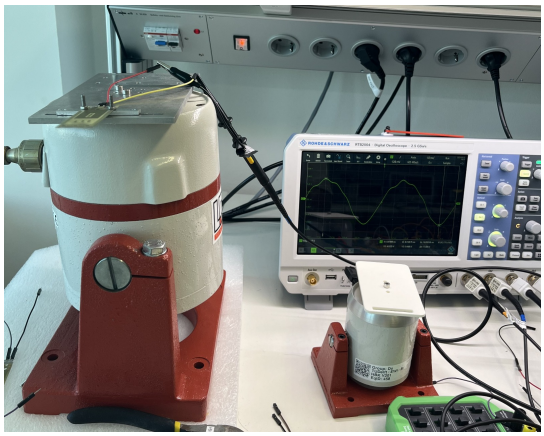

(b) Setup of Shaker

Figure A.3: Experimental setup from two perspectives

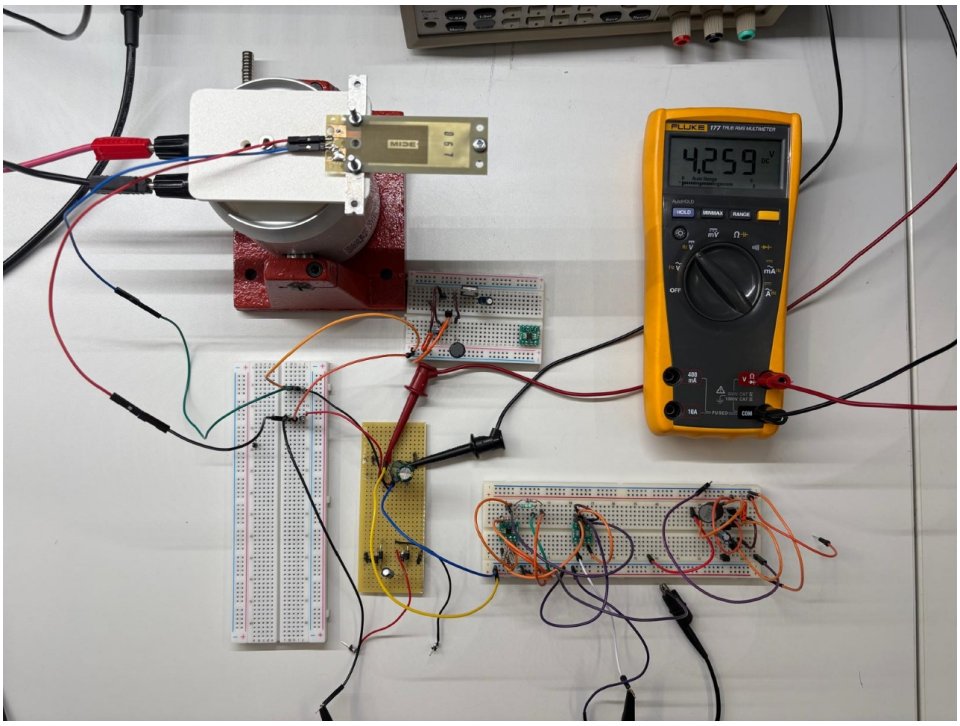

Figure A.4: Setup of Experiment 2

A.4. Energy Consumption Calculations

A.4.1. Energy Consumption of Sensor Transmission

To estimate the energy consumed by the sensor during a transmission, the following values are assumed:

- Regulated output voltage: $V = 3.3$ V
- **Single transmission:** $I = 4.9$ mA, $t = 332$ ms $= 0.332$ s
- **Burst transmission:** $I = 12$ mA, $t = 176$ ms $= 0.176$ s

The energy consumed for each case is:

$$E_{\text{single}} = V \cdot I \cdot t = 3.3\ \text{V} \cdot 4.9 \times 10^{-3}\ \text{A} \cdot 0.332\ \text{s} \approx 5.37\ \text{mJ}$$
$$E_{\text{burst}} = V \cdot I \cdot t = 3.3\ \text{V} \cdot 12 \times 10^{-3}\ \text{A} \cdot 0.176\ \text{s} \approx 6.97\ \text{mJ}$$

A.5.2. Energy Storage in the Capacitor

The energy stored in a capacitor is given by:

$$E = \frac{1}{2} C V^2$$

With:

- Capacitance: $C = 680\ \mu\text{F} = 680 \times 10^{-6}\ \text{F}$
- Full charge voltage: $V = 5.5\ \text{V}$

$$E_{\text{cap}} = \frac{1}{2} \cdot 680 \times 10^{-6}\ \text{F} \cdot (5.5\ \text{V})^2 \approx 10.3\ \text{mJ}$$

B

B.1. Noise

B.1.1. Python Code for Noisy Input Signal

The following Python code was used to generate a 58 Hz sine wave with added band-limited white noise to simulate realistic electromagnetic interference conditions for testing.

```
import numpy as np
import matplotlib.pyplot as plt

Fs = 16000           # Sampling rate (16 000 samples/sec)
duration = 1.0       # Duration = 1 second
N = int(Fs * duration)  # Total samples = 16 000
t = np.linspace(0, duration, N, endpoint=False)

#Sine wave
sine_wave = np.sin(2 * np.pi * 58 * t)

#Generate white noise and band-pass filter between -10300 Hz via FFT
noise = np.random.randn(N)
noise_fft = np.fft.rfft(noise)
freqs = np.fft.rfftfreq(N, 1 / Fs)

band_mask = (freqs >= 10) & (freqs <= 300)
filtered_noise_fft = noise_fft * band_mask
filtered_noise = np.fft.irfft(filtered_noise_fft, n=N)

#Scale noise to 0.2 of noise amplitude
noise_amplitude = 0.6
filtered_noise = filtered_noise / np.max(np.abs(filtered_noise)) * noise_amplitude

#sine + noise
composite_wave = sine_wave + filtered_noise

#normalzie to +-1
composite_wave /= np.max(np.abs(composite_wave))

#Save to CSV
filename = "58_0_6_amp.csv"
np.savetxt(filename, composite_wave, delimiter=",")

plt.figure(figsize=(8, 3))
plt.plot(t[:int(Fs)], composite_wave[:int(Fs)])
plt.title("58 Hz Sine + -10300 Hz Noise")
plt.xlabel("Time (s)")
plt.ylabel("Amplitude (normalized)")
plt.grid(True)
plt.tight_layout()
plt.show()

```

```
print(f"Waveform saved as '{filename}' with {N} samples at {Fs} Hz sampling rate.")
```

Listing B.1: Sine wave with band-limited noise